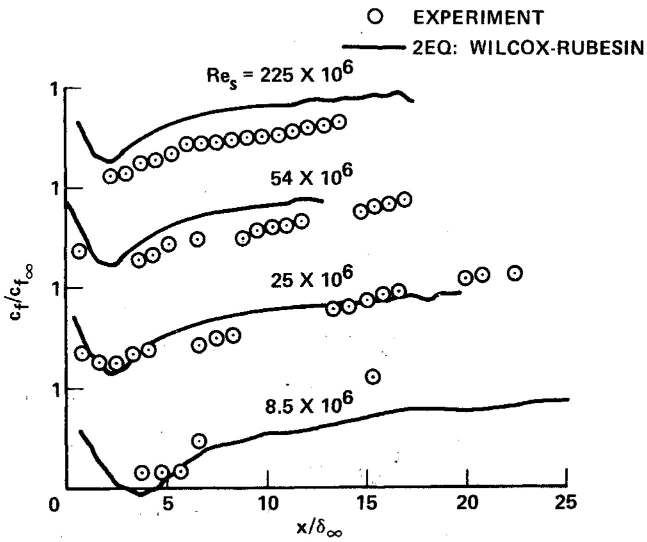

Fig. 5 Effect of Reynolds number on skin friction, $M_\infty = 1.42$.

calculations also illustrate these trends and indicate that the flow is separated for the lowest Reynolds number. Again, separation could not be confirmed with either the c_f or the flow direction data.

Conclusions

The results of the present investigation illustrate the sensitivity of the normal shock-wave/turbulent boundary-layer interaction to variations in Mach and Reynolds number for this flow. The Wilcox-Rubesin turbulence model provides a good representation of these effects for both the wall pressure and skin friction.

References

[1] Seddon, J., "The Flow Produced by Interaction of a Turbulent Boundary Layer with a Normal Shock Wave of Strength Sufficient to Cause Separation," ARC R&M No. 3502, March 1960.

[2] Mateer, G. G., Brosh, A., and Viegas, J. R., "A Normal-Shock-Wave Turbulent Boundary-Layer Interaction at Transonic Speeds," AIAA Paper 76-161, Washington, D.C., Jan. 1976.

[3] Viegas, J. R. and Horstman, C. C., "Comparison of Multi-equation Turbulence Models for Several Shock Separated Boundary-Layer Interaction Flows," AIAA Paper 78-1165, Seattle, Wash., July 1978.

[4] Wilcox, D. C. and Rubesin, M. W., "Progress in Turbulence Modeling for Complex Flowfields," NASA TP-1517, 1980.

[5] McDevitt, J. B., Levy, L. L., Jr., and Deiwert, G. S., "Transonic Flow About a Thick Circular-Arc Airfoil," AIAA Paper 75-878, Hartford, Conn., June 1975.

[6] Mateer, G. G. and Viegas, J. R., "Effect of Mach and Reynolds Numbers on a Normal Shock-Wave/Turbulent Boundary-Layer Interaction," AIAA Paper 79-1502, Williamsburg, Va., July 1979.

J80-196

00001
00006
20007

Downwash Impingement

B. N. Pamadi*
Indian Institute of Technology, Bombay, India

Introduction

WHEN operating over unprepared terrain, VTOL configurations are known to raise appreciable dust and debris. This not only results in loss of visibility for the pilot but also structural damage to propeller or engine compressor blading when they are hit by the sand particles or gravel lifted from the ground by the downwash impingement (Fig. 1).

Kuhn's studies[1] have shown that the bulk of the erosion or entrainment occurs close to the stagnation point and is confined to a region where the local surface dynamic pressure ($\frac{1}{2}\rho U^2$) exceeds a critical value. For dry sand and loose dirt, he finds that the critical surface dynamic pressure ranges 50-150 N/m^2. The dynamic pressure on the surface rises from zero at the stagnation point to a peak ($\frac{1}{2}\rho U_m^2$) at a point where the static pressure gradient vanishes and then starts falling off due to viscous decay (Fig. 1a). The conditions for incipient erosion are thus determined at the location of peak surface dynamic pressure. Kuhn's observations also reveal that the larger particles are predominantly rolled along the surface while the smaller ones are lifted from the ground.

The sand or dirt particles which are entrained are initially immersed in the boundary layer of the ground. The rolling of the particles occurs when the aerodynamic drag D exceeds the frictional force μW (drag entrainment) and the raising from the ground occurs if the aerodynamic lift L exceeds the particle weight W (lift entrainment). The particles develop lift because they are subjected to shear flow in the boundary layer.

For downwash flow with a uniform velocity distribution, Vidal[2] has developed some criteria for predicting lift and drag entrainment. His results are based upon the classical stagnation point boundary layer solution,[3] applicable to an uniform impinging flow of infinite extent. However, the downwash flow on leaving the jet nozzle has spread and decay characteristics similar to those of a free turbulent jet. In view of this, Vidal's analysis is restricted to low operating heights where the jet mixing effects are small and the velocity is nearly uniform (potential core). The experimental investigations of free jet impingement on normal surface also show that the classical stagnation point solution is applicable only to a small region around the stagnation point.[4,5] Reference 6 reports a more accurate solution for the ground boundary layer in the jet impingement region. Based upon this solution, Vidal's entrainment criteria are extended and presented here in a form applicable for any operating height above the ground surface. These results are in reasonably good agreement with Kuhn's experimental findings.

Criteria for Particle Entrainment

Vidal has given the following criteria,

Drag entrainment:

$$\frac{\rho_s g \delta_0}{\frac{1}{2}\rho U^2} \le \frac{3}{2\sqrt{2}} C_D \left(\frac{u_0}{U}\right)^2 \left(\frac{\delta_0}{a}\right) \tag{1}$$

where $D/W \ge \mu$, $\mu = 1/\sqrt{2}$, and $C_D = 0.5$.

Lift entrainment:

$$\frac{\rho_s g \delta_0}{\frac{1}{2}\rho U^2} \le \frac{u_0}{U}\left[\frac{9}{32}\frac{\delta_0}{a}\frac{u_0}{U} + 0.6723\frac{\delta_0}{U}\frac{du_0}{dz}\right] \tag{2}$$

where $L \ge W$ and $W = 4\pi/3\, \rho_s g a^3$.

The quantity $\rho_s g \delta_0 / \frac{1}{2}\rho U^2$ has been termed the loading parameter by Vidal and the same definition will be continued here. This definition of loading parameter is based upon the local dynamic pressure. Hence the loading parameter assumes an infinite value at stagnation point and decreases steadily outward. This parameter can be redefined in terms of maximum surface dynamic pressure ($\frac{1}{2}\rho U_m^2$), which is also equal to dynamic pressure on the free jet axis at an upstream distance, ($z = Z_\infty$) where the effect of the ground surface is negligible. This has the advantage that not only the loading parameter becomes constant with respect to radial distance,

Received May 29, 1979; revision received Nov. 30, 1979.

Index categories: Jets, Wakes, and Viscid-Inviscid Flow Interactions; Aerodynamics; Configuration Designs.

*Assistant Professor, Dept. of Aeronautical Engineering.

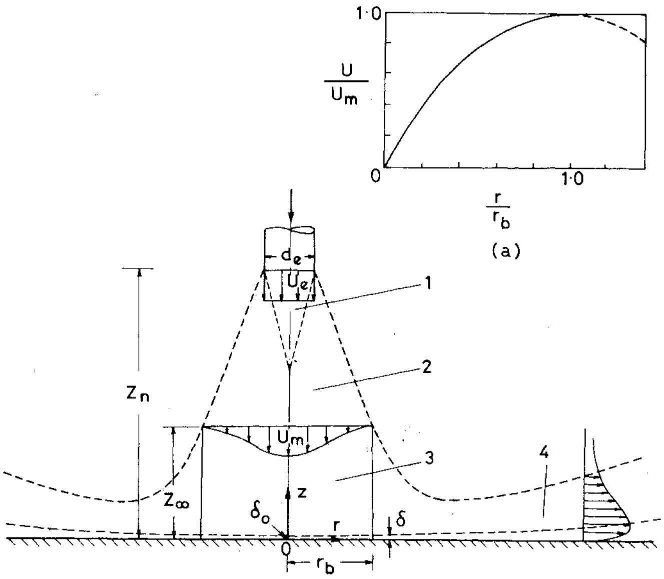

Fig. 1 Schematic diagram. 1-Potential core, 2-developed jet flow, 3-impingement region, 4-wall jet region.

but also that it can be expressed as a function of operating height (Z_n) of the VTOL configuration. Hence Eqs. (1) and (2) can be rewritten as,

$$\frac{\rho_s g \delta_0}{\rho U_m^2/2} \leq \frac{3C_D}{2\sqrt{2}}\left(\frac{U}{U_m}\right)^2\left(\frac{u_0}{U}\right)^2\left(\frac{\delta_0}{a}\right) \tag{3}$$

and

$$\frac{\rho_s g \delta_0}{\rho U_m^2/2} \leq \frac{u_0}{U}\left(\frac{U}{U_m}\right)^2\left[\frac{9}{32}\frac{\delta_0}{a}\left(\frac{u_0}{U}\right)+0.6723\left(\frac{\delta_0}{a}\right)\frac{\mathrm{d}u_0}{\mathrm{d}z}\right] \tag{4}$$

The functions δ_0, U/U_m, u_0/U, and $\mathrm{d}u_0/\mathrm{d}z$ are taken from the results reported in Ref. 6. Using these results, the right-hand sides of Eqs. (3) and (4) are evaluated for prediction of incipient entrainment, described below. Also the loading parameter can be expressed as a function of U_e, d_e, and Z_n as given in the following,

$$\frac{\rho_s g \delta_0}{\frac{1}{2}\rho U_m^2} = \frac{0.460\rho_s g d_e}{\frac{1}{2}\rho U_e^2\sqrt{Re_D}}\left(0.18\frac{Z_n}{d_e}+0.46\right)^3 \tag{5}$$

where $Re_D = U_e d_e/\nu$.

According to Ref. 6, Eq. (5) is applicable for such nozzle heights above the ground where the downwash airstream is fully developed prior to impingement. In Kuhn's[1] experiment this height was just equal to one diameter. But the above formulas based upon Abramovitch[7] data, are applicable for $Z_n/d_e \geq 4$. This apparent discrepancy is due to different lengths of the potential core. In Kuhn's measurements, the boundary layer thickness and the turbulence intensity at the nozzle exit must be so large that the potential core is consumed within a downstream distance of just one diameter. Another interesting point to observe in Kuhn's study is that although the propeller or ducted fan slipstream had a highly distorted velocity distribution at the exit, the spread and decay characteristics were similar to a free jet. Thus Eq. (5) can be employed for air nozzle, propeller, or ducted fan slipstream by taking care to use that value of Z_n/d_e where the actual centerline velocity of the slipstream is equal to that given by Abramovitch.[7] For small separation distances where the downwash stream is nearly uniform, the analysis given by Vidal can be used.

Criteria for Incipient Entrainment

The conditions for incipient entrainment are contained at the radial location where the right-hand side of Eq. (3) or (4) assumes a maximum. This quantity was calculated at radial distances from $r/r_b = 0.1$-1.0 and was plotted. From this exercise it was found that both the maximum values of lift and drag entrainment occur at the same radial station $r/r_b = 0.6$. These results and Vidal's criteria are presented in Fig. 2. We observe that there are two mechanisms for entraining ground particles. For small particles ($a/\delta_0 \leq 0.9$), the lift mechanism will cause incipient erosion and for large particles ($a/\delta_0 \geq 0.9$), it will be the drag mechanism.

For various combinations of U_e, d_e, and Z_n, Kuhn has measured the surface dynamic pressures when the incipient entrainment occurs. He conducted experiments on three different VTOL configurations, 2.54 and 10.16 cm diameter air nozzles and a 40.64 cm diameter ducted fan. The terrain specimen consisted of particles of various sizes ranging 0.007-0.13 cm diameter, mixed in various proportions. His results are also shown in Fig. 2 for comparison.

We observe from Fig. 2 that for the ducted fan, the incipient erosion is very well predicted by the present criteria. The agreement between the two results is reasonably good. However with the 2.54 and 10.16 cm air nozzles, the incipient erosion occurs at much lower values of the loading parameter than predicted by present criteria. A possible explanation for

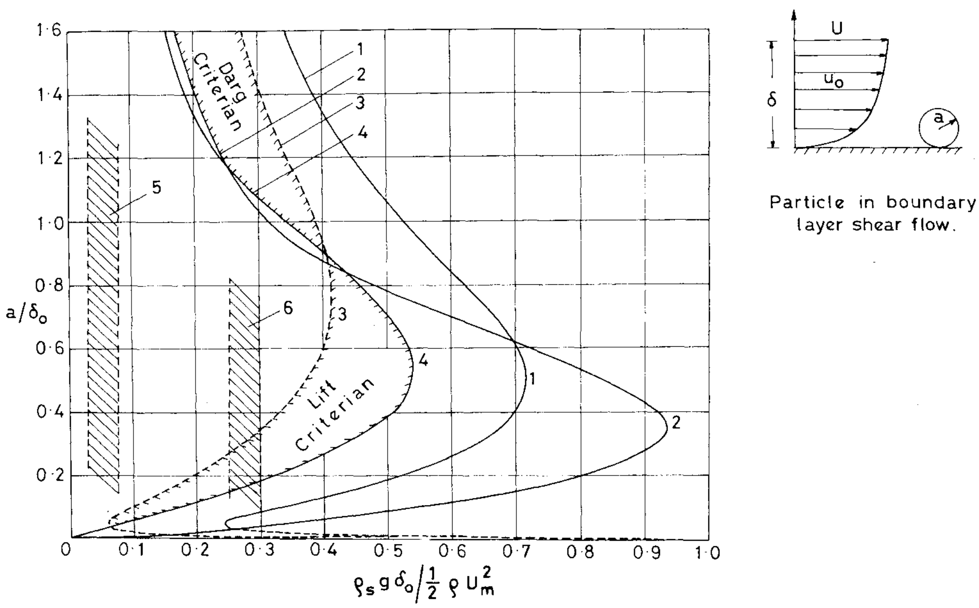

Fig. 2 Entrainment criteria. 1 and 2-Vidal's drag and lift crieteria, respectively, 3-drag criterion, 4-lift criterion, 5-Kuhn's air nozzle experiments, 6-Kuhn's ducted fan experiments.

this difference is that the boundary layer was too thin (0.02-0.08 cm). As a result, only a few particles were fully immersed in the boundary layer and the majority of the particles projected well outside. Moreover, the small particles which were fully immersed and could have been normally entrained due to lift are surrounded by larger ones and hence are protected to some extent from being displaced. This in turn necessitates larger surface dynamic pressures to dislodge them, resulting in a lower loading parameter. However, in practice, the VTOL configurations are many times larger than the 40.64 cm ducted fan and hence the boundary layer thickness can be such that bulk of the terrain particles can be fully immersed in it. Hence, the present criteria can be expected to give reasonably good results.

References

[1] Kuhn, R. E., "An Investigation to Determine Conditions under which Downwash from VTOL Aircraft Will Start Surface Erosion from Various Types of Terrain," NASA TN D-56, Sept. 1959.

[2] Vidal, R. J., "Aerodynamic Processes in the Downwash Impingement Problem," *Journal of the Aerospace Sciences*, Vol. 29, Nov. 1962, pp. 1067-1075.

[3] Schlichting, H., *Boundary Layer Theory*, Sixth Ed., McGraw-Hill Book Co., New York, 1968, pp. 87-92.

[4] Tani, I. and Komatsu, Y., "Impingement of Round Jet on Flat Plate," *XI International Conference on Applied Mechanics*, Munich, Springer-Verlag, Berlin, 1964, pp. 672-676.

[5] Hrycak, P., Lee, D. T., Gauntner, J. W., and Livingwood, N. B., "Experimental Flow Characteristics of a Single Turbulent Jet Impinging on a Flat Plate," NASA TN D-5690, March 1970.

[6] Pamadi, B. N. and Belov, I. A., "A Solution for the Mean Flow Parameters in the Impingement Region of a Free Jet on a Normal Flat Plate," *Journal of Aeronautical Society of India*, to be published.

[7] Abramovitch, G. N., *Theory of Turbulent Jets*, MIT Press, Cambridge, Mass., 1963.

J80-197

60009
40004
40007

Optimal Design of Ring Stiffened Cylindrical Shells Using Multiple Stiffener Sizes

Michael Pappas* and Jacob Moradi†
New Jersey Institute of Technology, Newark, N.J.

Introduction

KUNOO and Yang[1] investigated minimum weight cylindrical shells stiffened with both multiple size "I"-type rings and stringers using discrete stiffener buckling theory. They obtained a savings in weight of about 5% with the use of two ring and two stringer sizes for the example studied. Approximation methods are employed to reduce the computational effort required to approach a solution within reasonable bounds on cost (about 2000 s on a CDC 6500). Oddly, no mention is made in their work of the coalescence of buckling modes, a characteristic of optimal designs controlled by buckling behavior. Furthermore, their procedure apparently does not consider this situation.

This Note studies a "T"-type ring-stiffened shell problem by direct optimization without use of approximations or limitations in the number of stiffener sizes like those used in Ref. 1. The optimization formulation and procedure used here admit a large number of simultaneous buckling modes, thus allowing optimization under conditions of mode coalescence.

Received April 26, 1979; revision received Dec. 13, 1979.

Index categories: Structural Design; Structural Stability; Marine Vessel Design (including Loads).

*Associate Professor, Dept. of Mechanical Engineering.

†Research Associate, Dept. of Mechanical Engineering; presently, Body Engineer, Structural Analysis Dept., Chrysler Corp., Detroit, Michigan.

Procedure

The variables employed for this problem are skin thickness and ring dimensions and spacing. Each ring size used introduces a variable set associated with its dimensions. Thus, the number of variables is dependent on the number of sizes employed. To reduce problem dimensionality in this preliminary study, it is useful to introduce several assumptions. It is assumed that the shell is symmetrical with respect to a plane at midshell normal to the cylinder axis, that the ring flange thickness is equal to the web thickness, and that the flange width and web height are set at the maximum permitted to prevent local flange or web buckling.[2] It is shown in Ref. 2 that these assumptions have little effect on the optimal structural weight. The resulting problem variables as shown in Fig. 1.

Constraints on ring and skin yielding are applied in a fashion similar to Ref. 2 except that here a separate constraint must be considered for each shell panel. To determine the buckling pressures for the range of parameters of interest in this study, one could prudently examine all mode combinations where n (the number of circumferential waves) ranges from 0 to 20 and m (the number of axial half-waves) from 1 to 40. Using the analytical procedure of Refs. 3 and 4, this would involve the solution of several hundred eigenvalue problems of rank 840 (21×40) during a single optimization run. It may be seen, however, from an examination of the equations of Ref. 3 that for the case of uniform stiffeners the buckling modes are uncoupled with respect to n and interact only with respect to even or odd m. Thus, a single 840×840 problem can be reduced to a series of forty-two 20×20 problems substantially reducing computational effort required to determine buckling behavior. Furthermore, since most constraint function evaluations are for very similar designs, computational effort may be again reduced by restricting the range of odd or even m terms included in the formulation of the eigenvalue problem for a particular n based on a knowledge of the range necessary to include all m terms making a significant contribution. Likewise, only those n values which appear to be "critical" with respect to buckling need be examined.

Thus, let v^s_{mn} be the value of an element of the matrix of eigenvectors which represents the buckling behavior of the design x^s, and m^s_n be the value of m associated with the largest value of the component v^s_{mn} of vector v^s_n. Now, using the procdure of Ref. 3 starting from $n = n_{\min}$, where $n_{\min}$ is the lowest n considered, and setting an index $i = 1$, set up and solve an M by M eigenvalue problem P^s_n for design x^s using terms associated with

$$m = m_{\min}, \quad m_{\min} + 2, \quad m_{\min} + 4, \ldots, m_{\max} \tag{1}$$

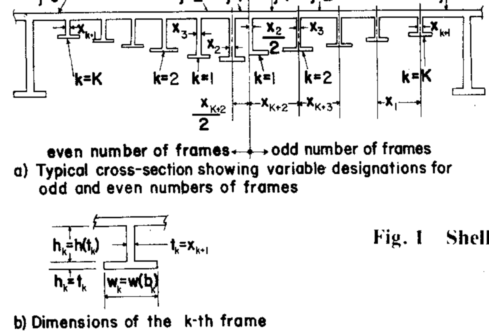

a) Typical cross-section showing variable designations for odd and even numbers of frames

b) Dimensions of the k-th frame

Fig. 1 Shell design variables.